AIAA JOURNAL
Vol. 36, No. 9, September 1998

Unsteady Vortex Structure over Delta-Wing Subject to Transient Along-Core Blowing

Cheng-Hsiung Kuo* and Ni-Yu Lu†
National Chung Hsing University, Taichung 40227, Taiwan, Republic of China

Unsteady vortex structure over a delta-wing in response to the transient along-core blowing is investigated by velocity measurements and the phase-trigger technique. The wing geometry has a 75-deg sweep angle and is at a 40-deg angle of attack. The changes of the along-core and the swirling velocity components are related to illustrate the evolution of the vortex structure when the transient blowing is applied along the axis of the vortex core. It is found that the highly sensitive character of the central region of the vortex core occurs not only in the along-core direction but also in the circumferential direction. Within the stable vortex core, the along-core velocity in response to the transient along-core blowing must change in accordance with the swirling velocity. The magnitudes of the along-core and the swirling velocity components within the stable vortex core must satisfy the stability parameter and the limitation of the maximum swirl angle. The maximum swirl angle within the stable vortex core is nearly the same both in the case of transient along-core blowing and in the unperturbed case. When the transient along-core blowing is introduced, increasing magnitudes in both the along-core and the swirling velocity components tend to enlarge the favorable pressure gradient along the vortex center. This leads to the substantial delay of the vortex breakdown location.

Nomenclature

A_p	= area of the blowing slot
A_w	= area of the half delta-wing
C	= root chord of the wing, 20 cm
C_μ	= blowing coefficient, $(V_p/U_\infty)^2\,(A_p/A_w)$
Dy	= diameter of the vortex core in spanwise direction in Fig. 4
Dz	= diameter of the vortex core in direction normal to wing surface in Fig. 4
p_c	= pressure at the vortex center
p_s	= pressure on the wing surface
q	= stability parameter, $w_{\max}/(u_{\max} - U_\infty)$
R_c	= radius of the vortex core, $(Dy + Dz)/4$
r^*	= dimensionless radial distance from the vortex center, r/R_c
S_o	= semispan at $X/C = 1.0$
s	= local semispan
t^*	= dimensionless time, tU_∞/C
U_∞	= freestream velocity, 15 cm/s
u^*	= dimensionless along-core velocity, u/U_∞
u_c^*	= dimensionless centerline velocity, u_c/U_∞
V_p	= velocity at the exit of the blowing slot
w^*	= dimensionless swirling velocity, w/U_∞
X, Y, Z	= laboratory coordinate in Fig. 2
x, y, z	= coordinate system fixed on the vortex core in Fig. 2
x^*	= dimensionless streamwise distance, x/C
α	= angle of attack of the wing
β	= angle of vortex core from the platform
θ	= angle of vortex core above the wing surface
Λ	= sweep angle of the wing
ϕ	= swirl angle, $\tan^{-1}(w/u)$
φ	= circumferential direction in Fig. 2b

Introduction

THE subject of the unsteady vortex characteristics over highly swept delta-wings has been of great research interest especially at high angles of attack (AOA) during the past few decades. The conical leading-edge vortices over delta-wings define a large vortex lift that allows supermaneuvering over a wide range of AOA. Delay of the vortex breakdown location and the reorganization of the vortex structure are the main goals for achieving supermaneuverability and agility in the poststall range of AOA.[1–3]

Active controls of the vortex structure over delta-wings do create large vortex lift at high AOA. Qualitatively, Shi et al.[4] demonstrated that the length of the vortex core, before breakdown, can be effectively enlarged by proper arrangements of the blowing location and the orientation. The wind-tunnel experiments by Bradley et al.[5] and Campbell[6] also found a large increase in lift at high AOA as the vortex core is perturbed by spanwise blowing. Application of unsteady blowing and suction in the direction tangent to the leading edge was performed by Gu et al.[7] They found that the onset location of vortex breakdown is a strong function of perturbation frequency. In their results, the most effective frequency of the alternate suction-blowing perturbation was around U_∞/C (the inverse of the convection timescale). When perturbed at this frequency, the vortical structure over the delta-wing is reorganized, and the onset location of vortex breakdown is delayed substantially. Recently, blowing applied at the trailing edge of a delta-wing was conducted by Helin and Watry.[8] In a vertical water channel, Lee et al.[9] investigated the vortex breakdown phenomenon over a delta-wing in a well-controlled time-varying freestream. Their results showed that the vortex breakdown location moved upstream during the flow acceleration and vice versa during the flow deceleration. The aforementioned investigations are all focused on the static delta-wing in steady or unsteady flows.

For the delta-wing undergoing pitching motion, Magness et al.[10] and Cipolla and Rockwell[11] investigated by experiment the controllability of the vortex breakdown location. They found that the coherence of the leading-edge vortex is promoted during the pitch-up motion. However, the vortex structure is close to that over the static delta-wing during the pitch-down motion. This characteristic was observed for a range of pitching rates. On the other hand, the numerical simulation of Visbal and Gordnier[12] showed that a higher pitch rate will result in a significant delay of the vortex breakdown location at high AOA. This result can be even more pronounced when the pitch axis is located at the trailing edge. More recently, Vorobieff and Rockwell[13] controlled the vortex structure by applying a leading-edge flap and trailing-edge blowing simultaneously when the delta-wing underwent pitch motion. They found that the mean location of vortex breakdown can be extended by 100% using the multiple-control technique.

As stated in the review paper by Lee and Ho,[14] the vortex near the apex is more sensitive to the disturbance than any other locations along the leading edge. This leads to the recent studies of Kuo and Lu[15] and Kuo et al.[16] They attempted to explore the recovery of the

Received June 5, 1997; revision received April 21, 1998; accepted for publication April 21, 1998.

*Professor, Department of Mechanical Engineering.
†Graduate Assistant, Department of Mechanical Engineering.

vortex breakdown location and the response of the vortex core when small amounts of along-core blowing perturbation were introduced. In their studies, the delay of the vortex breakdown location, the dependence on the AOA, the blowing rate, and the blowing type were addressed. Furthermore, Kuo et al.[16] found that the central region of the vortex core is more sensitive to external perturbation in the along-core direction than the outer region. This key characteristic explains the transformation of the along-core velocity distribution from jet-like to wake-like profiles when the vortex breakdown location is encountered. Although the location of vortex breakdown can be delayed by 80% through transient along-core blowing, the detailed evolution characteristics of the vortex core in response to transient blowing are not yet understood completely.

Consequently, the objective of this study is to understand the time-dependent characteristics of the vortex structure over a highly swept ($\Lambda = 75$ deg) delta-wing at high AOA ($\alpha = 40$ deg). It includes the time-dependent variations of the along-core and the swirling velocity components in response to the transient along-core blowing issued from the wing apex. Moreover, the variations of the pressure gradient along the vortex center will be addressed in connection with the evolution of the swirling velocity.

Experimental Setup and Measurement Techniques

Flow Conditions and Model Setup

All experiments were performed in a low-speed recirculating water channel. The turbulence intensity is reduced to a level of 0.42% at $Re_C = 3.06 \times 10^4$. Moreover, the nonuniformity of the freestream velocity distribution is around 1.2%. As shown in Fig. 1a, the half delta-wing has a 75-deg sweep angle and is beveled upward at an angle of 25 deg, forming a sharp leading edge. The model of the half delta-wing is mounted on the platform having a leading edge of 5:1 elliptic profile (Fig. 1a). The combination of the half delta-wing and the platform simulates the actual wing–fuselage arrangement. The full-span platform is placed horizontally about 5 cm above the bottom of the channel, allowing uniform inflow with zero incidence angle relative to the platform. The blockage ratio is 0.028 at AOA = 40 deg when the half delta-wing is mounted on the platform. The momentum coefficient is selected to be $C_\mu = 0.088$. Figure 1b shows the use of a rotating circular disk to align the along-core blowing direction with the axis of the primary vortex core. The blowing slot, having a 0.5-mm diameter, is drilled through the thickness of the horizontal platform along the vortex core direction that is predetermined from the dye-colored flow visualization of the vortex core. The transient along-core blowing takes the form of a finite impulse lasting for $0.6C/U_\infty$ and suddenly terminates afterward. Detailed

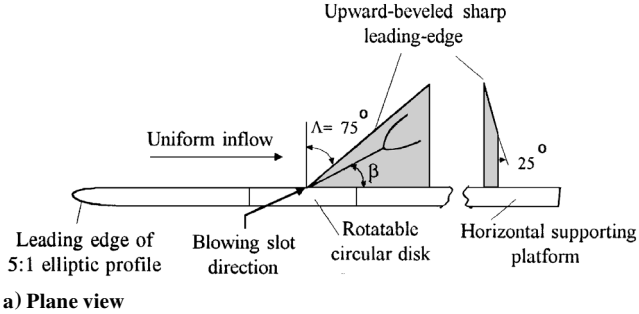

a) Plane view

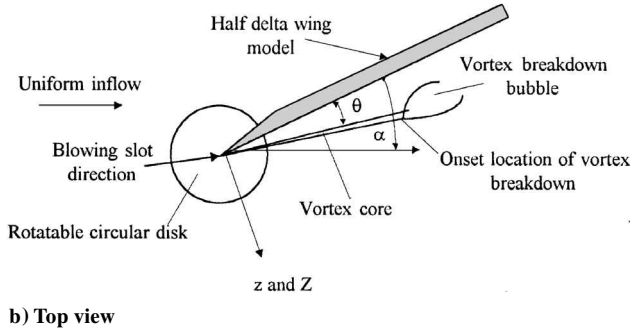

b) Top view

Fig. 1 Experimental setups of the half delta-wing model mounted on the full-span horizontal platform.

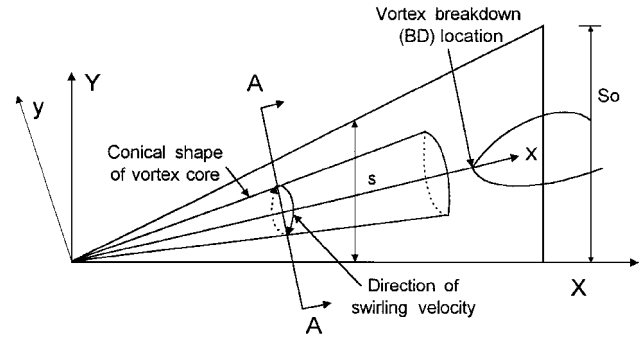

a) Plane view representation of the vortex core (Cartesian)

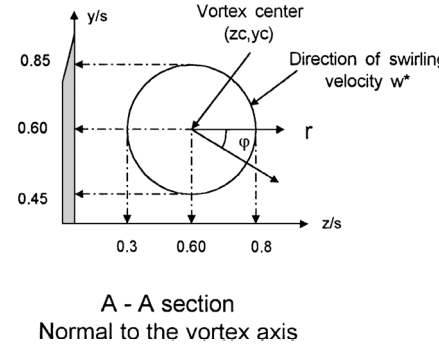

b) Cross-sectional representation of the vortex core (polar)

Fig. 2 Coordinates of the vortex core system.

information about the alignments of the along-core blowing direction and the personal-computer-based blowing control device can be found in Refs. 16 and 17.

Coordinate Systems

With the wing apex as the origin, the coordinate systems are defined in Fig. 2. The positive x and y, in Fig. 2a, denote the directions along and normal to the axis of the primary vortex core, respectively. However, the X/C denotes the streamwise distance measured from the origin (or the wing apex) as a fraction of the root chord C. The direction of positive z denotes the distance away from the wing surface, and s represents the local semispan at any X/C location. As depicted in Fig. 2a, the velocity measurements (both the along-core and the swirling components) are taken on the A–A cross section that is normal to the axis of the vortex core. Figure 2b shows the enlarged illustration of the A–A cross section of the vortex core in the polar coordinate system centered at (z_c, y_c). The coordinates in Fig. 2a are used to define the onset location of vortex breakdown. However, the coordinates in Fig. 2b are used to illustrate the evolution of the along-core and the swirling velocity components within the vortex core.

Velocity Measurements and Phase-Trigger Technique

Velocity measurements of the along-core and the swirling components are performed by the nonintrusive laser Doppler anemometry (LDA) system and a precise traversing table of 1/100-mm accuracy. Under the specified flow and the blowing conditions, the velocity measurements are performed on several crossflow planes between $X/C = 0.3$ and 0.7. Depending on the size of the vortex core at different X/C locations, the number of measuring points on each plane ranges from 380 to 620 points to provide good spatial resolution. In the LDA velocity measurement, the photon density, the burst density, and the data density are all important characteristics to determine different types of output velocity signal. The photon density depends strongly on the emission rate and the responding time of the LDA system. For the LDA system used in the present study, the light flux at the output of the photomultiplier tube has a high photon density. In addition, the burst density is defined as the effective mean number of the particles coexisting within the measuring volume. When the flow is seeded with particles (TiO_2) having proper concentration, the Doppler burst contributed by many particles residing simultaneously within the measuring volume will overlap to output the velocity signal as a continuous function of time. The continuous

velocity signal, caused by the high photon and high burst density, is contaminated by the phase and ambiguity noise that can be minimized by the use of a low-pass filter. The data density is defined as the mean number of the validated data points passing the measuring volume per second. An efficient way to increase the data density is to increase the sampling rate (or frequency) in the signal processor. In the present study, the operational conditions of the LDA system fall into the region of high photon, high burst, and high data density. Therefore, a sufficiently high sampling rate, e.g., 650,000 Hz, the sample-and-hold characteristics, and the programmable bandwidth of the filter built in the signal processor (IFA 550) all ensure that the output (analog) velocity signal will be a continuous function of time. The data acquisition system placed downstream of the IFA 550 can digitize the continuous velocity signal with a sampling frequency of 200 Hz for postprocessing. Furthermore, the small size (8 μm) and fast responding time (6.2 μs) of the seeding particles relative to the water flow further ensure that the seeding particles will follow naturally the motion of the fluid. Other information on the LDA system can be found in Ref. 18.

The phase-trigger technique initiates the data acquisition at the onset instant of transient along-core blowing. It provides the same initial instant for all of the velocity measurements within the flow domain. This technique allows conversion of the temporal variations of the local velocity measured by the LDA system into the instantaneous spatial velocity distributions. This conversion, starting from the onset instant of transient along-core blowing, provides results that can be used to elucidate the time-dependent evolution of the flow structure and to explore some important characteristics of the vortex core.

Data Reduction Process

At each measuring location within the flow domain, the velocity time signals were taken for 10 sample experiments by the phase-trigger technique. As depicted in the block diagram in Fig. 3, the time signals are obtained by ensemble averaging the phase-triggered time signals out of the 10 sample runs at each specified location. Collections of the ensemble-averaged velocity time signals for all measuring points at the same instant yield the ensemble-averaged instantaneous crossflow velocity profile in Fig. 4. Figure 5 illustrates the ensemble-averaged time signals at the vortex center at successive X/C locations. The center locations and the radii R_c of the vortex core are depicted in Fig. 6 as functions of X/C. The ensemble-averaged time signals at each z/s location are shown in Fig. 7. Before the vortex breakdown location, the maximum uncertainty due to the ensemble-averaging process is around 2.14% within the vortex core. Throughout the complete evolutionary process, the centrifugal effect (CE) is evaluated from the ensemble-averaged instantaneous crossflow profiles of w^*.

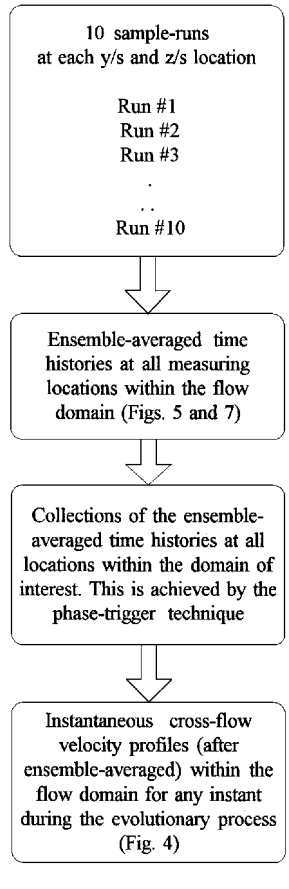

Fig. 3 Block diagram for the data reduction process.

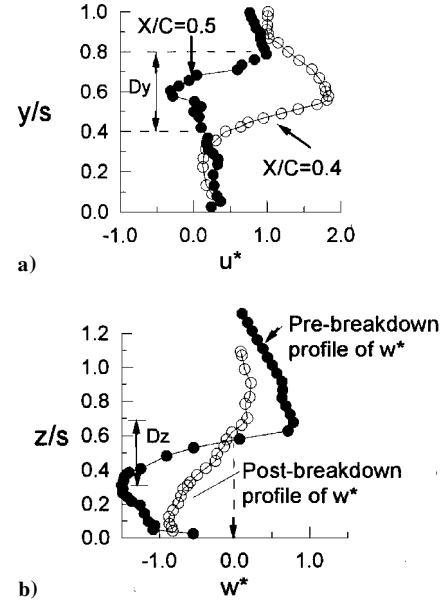

Fig. 4 Crossflow profiles (ensemble averaged) of a) the along-core velocity at $t^* = 0$ and at $X/C = 0.4$ and 0.5 and b) the swirling velocity profiles across the vortex core at the prebreakdown and the postbreakdown stages. All velocities are normalized by the freestream velocity. The ordinates y and z are normalized by the local span s.

Results and Discussion

Leading-Edge Vortex Structure Before Blowing

The crossflow distributions of u^* and w^* across the vortex core are shown in Fig. 4 to illustrate the flow structure at the prebreakdown and the postbreakdown stages. The abscissas are normalized by the freestream velocity U_∞. Before the transient along-core blowing starts ($t^* = 0$), the distribution of u^* at $X/C = 0.4$ in Fig. 4a shows a velocity-excess (or jet-like) profile, with a maximum overshoot near the vortex center ($y/s = 0.6$) denoting the prebreakdown vortex structure. On the contrary, the distribution of u^* exhibits a velocity-deficit (or wake-like) profile at $X/C = 0.5$, with a minimum magnitude near the vortex center ($y/s = 0.6$). This wake-like profile clearly indicates the already broken-down stage of the vortex core at $t^* = 0$. In Fig. 4b, the distribution of w^* across the vortex core at the prebreakdown stage resembles Burgers' vortex.[19] Considering an idealized point vortex, the location corresponding to the zero swirling velocity represents the center of the vortex core. In this experiment, the center of the leading-edge vortex is around $z/s = 0.6$ above the wing surface. In Fig. 4b, the distribution of w^* at the prebreakdown stage shows a significant gradient within $0.4 < z/s < 0.8$ across the vortex center. However, a significant reduction in the gradient of the w^* profile is found in the same region when the vortex core is at the postbreakdown stage. These profiles of w^* clearly indicate that the along-core vorticity is much stronger at the prebreakdown stage than at the postbreakdown stage.

Onset of Vortex Breakdown After Transient Along-Core Blowing

When the transient along-core blowing is issued from the wing apex, the ensemble-averaged time histories of u_c^* measured at the vortex center are shown in Fig. 5 at successive X/C locations. The abscissa denotes the dimensionless time t^* that begins from the onset instant of transient blowing. In Fig. 5, the magnitudes of all of the u_c^* increase drastically to a local maximum when the

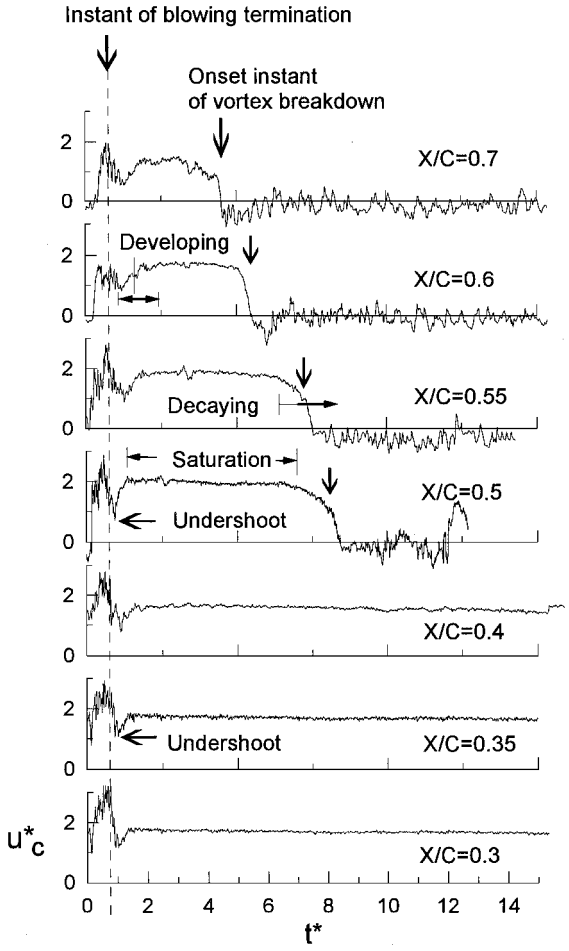

Fig. 5 Ensemble-averaged time histories of the along-core velocity measured at the vortex center for various streamwise *X/C* locations. Shown is the upstream movement of the vortex breakdown location after the transient along-core blowing terminates; $t^* = 0$ denotes the onset instant of transient blowing.

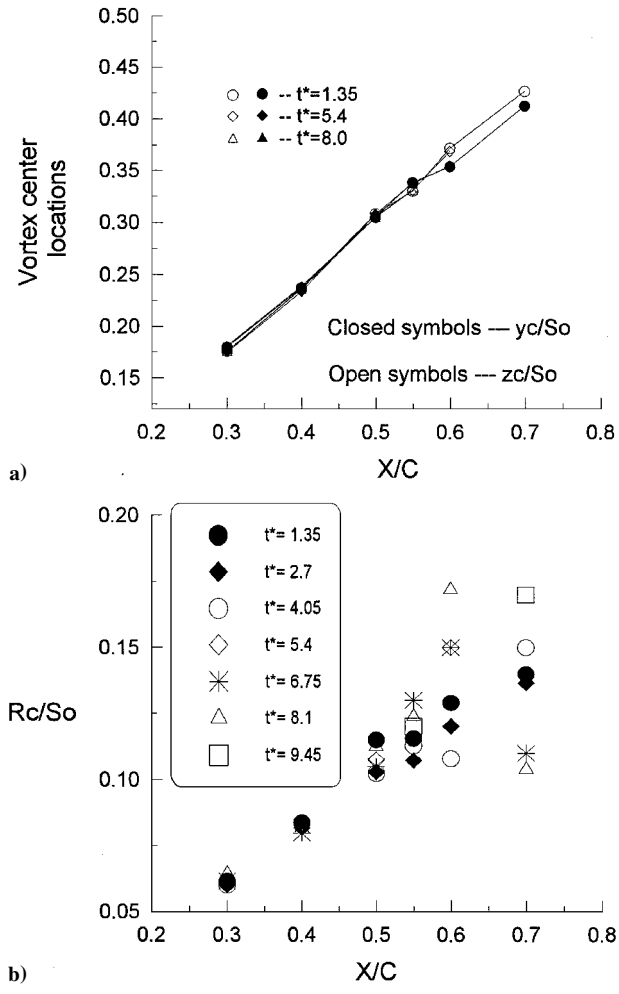

Fig. 6 Streamwise distributions of a) the vortex center location before the vortex core breaks down and b) the averaged radius R_c of the vortex core at different instants after the transient blowing terminates.

transient along-core blowing begins. Then the magnitude of u_c^* decreases rather rapidly to a local minimum, termed *undershoot*, after the transient along-core blowing terminates suddenly. Afterward, the vortex core exhibits the developing stage by increasing the magnitude of u_c^* from the undershoot. Following the developing stage, the magnitude of u_c^* maintains nearly constant values for different time intervals at different X/C locations. This is called the saturation stage. The time histories of u_c^* exhibit only the developing and the saturation stages at locations upstream of $X/C = 0.5$, where the vortex core never breaks down. Note that no sudden drop of u_c^* can be found upstream of $X/C = 0.5$ in Fig. 5. However, the developing, the saturation, and the decaying stages can be clearly distinguished from the time histories of u_c^* at locations $X/C \geq 0.5$. In the decaying stage, the magnitude of u_c^* decreases drastically to nonpositive mean values. Downstream of $X/C = 0.5$, the sudden drop in the magnitude of u_c^* corresponds exactly to the occurrence of the vortex breakdown. As marked by the vertical arrows, the sequential occurrence of the sudden drop from $X/C = 0.7$ back to $X/C = 0.5$ clearly shows the upstream movement of the vortex breakdown location after the transient along-core blowing terminates.

Conical Structure of Leading-Edge Vortex

To further understand the leading-edge vortex structure, we examined the center location (z_c, y_c) and the averaged radii R_c of the vortex core at some selected instants after the transient along-core blowing terminates. The y_c and z_c are the locations where the along-core velocity attains the maximum overshoot and the swirling velocity is zero. The R_c value is evaluated by $(D_y + D_z)/4$, where D_y and D_z are the core diameters shown in Figs. 4a and 4b, respectively. In Fig. 6a, the center locations of the vortex core before the vortex breakdown show a linear variation along the streamwise direction. The maximum deviation of y_c and z_c estimated from 10 sample runs is around 0.67%. When the dye is released from the wing apex, the linear relationship shown in Fig. 6a coincides well with the observed straight colored dye that represents the trajectory of the vortex center. Furthermore, the averaged radius R_c in Fig. 6b also exhibits a linear increase in the streamwise direction before the vortex core breaks down. Downstream of the breakdown location, a much larger deviation from the linear relationship is caused by the abrupt divergence of the vortex core. For the vortex core at the prebreakdown stage, the maximum deviation of R_c/S_o measured from 10 sample runs is about 1.26%. The results in Figs. 6a and 6b further point out that the leading-edge vortex structure is of conical shape and is nearly axisymmetric about the straight vortex axis.

Evolution of the Along-Core Velocity

The time histories of u^* across the vortex core will be briefly summarized to illustrate the evolution of u^* in relation to w^* (shown later) when the transient along-core blowing is applied. Before the along-core blowing is applied ($t^* = 0$ in Fig. 4a), the crossflow distribution of $u^*(y)$ initially has a velocity-deficit profile (namely, $u_c^* < 1.0$) at $X/C = 0.5$ that clearly indicates the already broken-down stage of the vortex core. In Fig. 5, the magnitude of u_c^* downstream of $X/C = 0.5$ increases from the undershoot to a higher value ($u_c^* = 1.5$–2.0) during the developing stage. After the developing stage, the magnitude of u_c^* reaches a plateau region of nearly constant magnitude ($u_c^* = 1.5$–2.0). During the developing and the saturation stages, the crossflow distribution of $u^*(y)$ exhibits a velocity-excess profile (or $u_c^* > 1$), indicating the stable vortex core. The transformation from the wake-like profile to the jet-like velocity profile across the vortex core implies that the vortex structure has been reorganized. Downstream of $X/C = 0.5$, the reorganization of the vortex

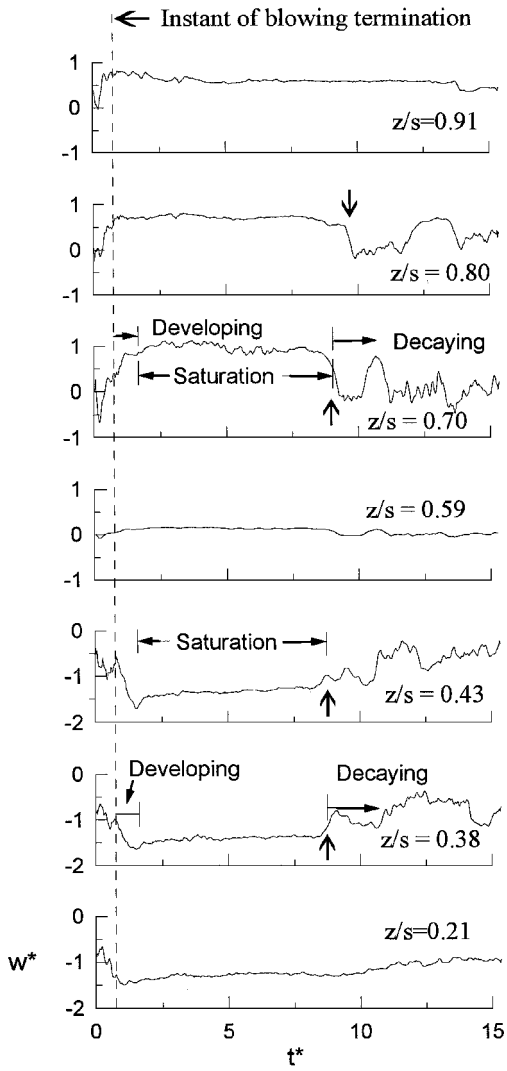

Fig. 7 Time histories of the swirling velocity at various *z/s* locations across the vortex core at *X/C* = 0.5. The term w^* is the dimensionless swirling velocity, t^* is the dimensionless time, and $t^* = 0$ indicates the onset instant of blowing. Vertical dashed lines denote the instant of blowing termination.

core clearly suggests that the onset location of vortex breakdown is effectively delayed farther downstream. In the decaying stage, the magnitude of u_c^* downstream of $X/C = 0.5$ reduces significantly below 1.0. During the decaying stage, the distribution of u^* has a tendency to become the wake-like profile, indicating the recovery of the vortex breakdown location during the decaying stage. The detailed characteristics of the evolution stages are described in Ref. 16.

Evolution of the Swirling Velocity

The results in Figs. 6a and 6b clearly show that the leading-edge vortex structure can be assumed to have a conical shape and be axisymmetric about the vortex center before the vortex core breaks down. When compared with the along-core and the swirling velocity components, the radial velocity component within the conical vortex core is about one order of magnitude smaller and can be neglected. Thus, the dimensionless continuity equation in polar coordinates (Fig. 2b) for incompressible fluid can be simplified as

$$\frac{\partial w^*}{r^* \partial \varphi} = -\frac{\partial u^*}{\partial x^*}\left(\frac{R_c}{C}\right) \tag{1}$$

Before vortex breakdown, all of the crossflow distributions of u^* have similar jet-like profiles[16] and can be expressed in a nondimensional functional form:

$$u^*(x^*, r^*, t^*) = 1 + f(x^*)g(t^*)\exp(-r^{*2}) \tag{2}$$

Substituting Eq. (2) into Eq. (1) and integrating with respect to φ yields the swirling velocity component. Thus, the time rate of change of w^* can be expressed as

$$\frac{\partial w^*}{\partial t^*} = -\frac{\partial}{\partial t^*}\int_0^{\varphi} r^* \frac{\partial u^*}{\partial x^*}\left(\frac{R_c}{C}\right) \mathrm{d}\varphi$$

$$= -\varphi\left(\frac{\partial f}{\partial x^*}\right)\left(\frac{\partial g}{\partial t^*}\right)\exp(-r^{*2})\left(\frac{r}{C}\right) \tag{3}$$

Over the complete evolutionary stages shown in Fig. 5, all of the time histories of u_c^* in the region $X/C < 0.5$ reveal the character $\partial u_c^*/\partial x^* \approx 0$ within the vortex core. Downstream of $X/C = 0.5$, the time histories of u_c^* show $\partial u_c^*/\partial x^* < 0$ within the vortex core. This gives $\partial f/\partial x^* \approx 0$ in the region $X/C < 0.5$ and $\partial f/\partial x^* < 0$ in the region $X/C \geq 0.5$ during the complete evolutionary process.

Within the central region of the vortex core at $X/C = 0.5$, the local velocity u^* increases with time during the developing stage. This gives the result $\partial g/\partial t^* > 0$. During the developing stage, substitutions of $\partial f/\partial x^* < 0$ and $\partial g/\partial t^* > 0$ into Eq. (3) give rise to the result $\partial w^*/\partial t^* > 0$ in the region $r = (z - z_c) > 0$ (namely, at $z/s = 0.7$ in Fig. 7). However, the opposite behavior $\partial w^*/\partial t^* < 0$ can be observed on the other side of the vortex center $r = (z - z_c) < 0$ (namely, at $z/s = 0.43$ and 0.38 in Fig. 7). During the saturation stage, both $\partial f/\partial x^* < 0$ and $\partial g/\partial t^* \leq 0$ lead to the result $\partial w^*/\partial t^* \geq 0$ in the region $r = (z - z_c) < 0$. After the developing stage, the plateau regions with small positive slope correspond to the saturation stage of the w^* component (at $z/s = 0.38$ and 0.43 in Fig. 7). Likewise, the plateau regions with small negative slope reveal the result $\partial w^*/\partial t^* \leq 0$ in the region $r = (z - z_c) > 0$ (that is, at $z/s = 0.70$ and 0.80 in Fig. 7) during the saturation. At the beginning of the decaying stage, the sudden drops of u^* imply that the crossflow distributions of u^* transform from the jet-like to wake-like profile. This also gives $\partial f/\partial x^* < 0$. Substitutions of $\partial f/\partial x^* < 0$ and $\partial g/\partial t^* < 0$ into Eq. (3) yield $\partial w^*/\partial t^* < 0$ on one side of the vortex center $r = (z - z_c) > 0$. However, on the other side of the vortex center $r = (z - z_c) < 0$, the time histories of w^* reveal the opposite result $\partial w^*/\partial t^* > 0$. Furthermore, the time history of w^* near the vortex center ($r \approx 0$ or $z/s = 0.59$) fluctuates randomly about zero. Similarly, the variations of the swirling velocity w^* in the outer region of the vortex core can also be analyzed by Eqs. (1–3). The results shown in Fig. 7 reveal that the highly sensitive character of the central region of the vortex core occurs not only in the along-core direction but also in the circumferential direction.

Stability Parameter and Maximum Swirling Angle

In Fig. 8, the streamwise variations of the stability parameter q are shown at selected instants after the transient along-core blowing terminates. In Fig. 8, the maximum deviation of q values out of 10 sample runs is around 1.21% before the vortex core breaks down. Downstream of the vortex breakdown location, the q values become negative and have maximum deviation about 7.6%. In the experiments performed by Faler and Leibovich[19] and the analysis of Lessen et al.,[20] the value of q must be greater than 1.5 to ensure the complete stabilization of the disturbances of all nonaxisymmetric modes. Upstream of $X/C = 0.5$, the q values vary between 2.1 and 1.8 for all instants throughout the evolutionary process. This indicates that the vortex core is stable upstream of $X/C = 0.5$. However, the stability parameter decreases to negative values as the vortex core breaks down. During the developing stage ($t^* \leq 1.35$) and the early part of the saturation stage ($1.35 \leq t^* \leq 2.7$), the q values vary around 1.9–2.1 within the range $0.3 < X/C < 0.7$. This implies that the vortex core in the region $X/C > 0.5$ is reorganized and the vortex breakdown location has been delayed downstream of $X/C = 0.7$ (refer to Fig. 5) for $1.35 \leq t^* \leq 2.7$. During the later part of the saturation stage ($t^* \geq 5.4$), the q value drops significantly near $X/C = 0.6$. The sudden drop of the q value clearly indicates the occurrence of vortex breakdown around $X/C = 0.6$ (marked by the open circle in Fig. 8). During the decaying stage, the location corresponding to the sudden drop of the q value moves progressively upstream toward the $X/C = 0.5$ location for $t^* > 9.45$.

Table 1 Variation of the maximum swirl angle ϕ_{max} within the vortex core after transient along-core blowing terminates

	$\phi_{max} = \max[\tan^{-1}(w/u)]$[a]					
X/C	0.3	0.4	0.5	0.55	0.6	0.7
$t^* = 1.35$	47.6	45.3	43.0	42.2	41.3	40.3
$t^* = 2.7$	46.3	44.2	42.9	41.1	40.2	39.8
$t^* = 4.1$	44.8	45.1	43.2	41.6	38.1	BD[b]
$t^* = 5.4$	44.9	44.8	43.8	38.9	BD	BD
$t^* = 6.75$	46.5	45.0	41.8	37.1	BD	BD
$t^* = 8.1$	46.5	44.8	42.2	38.7	BD	BD
$t^* = 9.45$	46.2	43.3	BD	BD	BD	BD

[a]The terms w and u are the swirl and the along-core velocity components measured within the vortex core; ϕ_{max} denotes the maximum swirl angles at the specified streamwise location, and the unit of ϕ_{max} is degrees.
[b]BD indicates the occurrence of the vortex breakdown location.

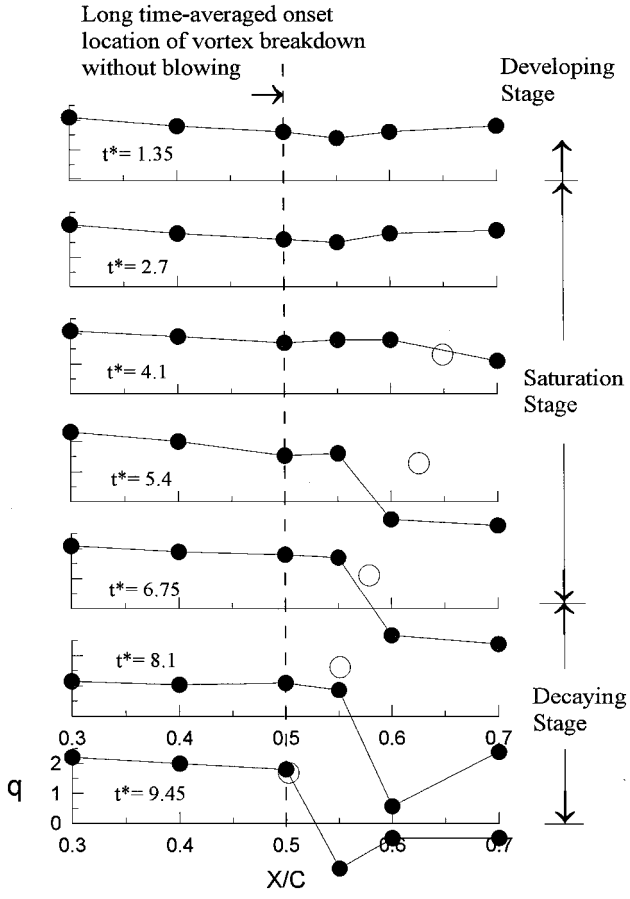

Fig. 8 Streamwise variations of the stability parameter q at different instants after the transient along-core blowing terminates. The ordinates are of the same scale. The open circles on each curve indicate the instantaneous onset locations of vortex breakdown obtained from flow visualization.

Before vortex breakdown, the maximum swirl angles ϕ_{max} obtained at different X/C locations are listed in Table 1 after the termination of the transient along-core blowing ($t^* \geq 1.35$). The maximum swirl angles are the averaged value from 10 sample runs with maximum deviation 2.3% before the vortex core breaks down. In Table 1, the maximum swirl angles before vortex breakdown are close to those obtained by Faler and Leibovich[19] for spiral-type breakdown (namely, between 43.8 and 46.0 deg). However, the maximum swirl angle ϕ_{max} reduces its magnitude as the vortex core is about to break down. The vortex breakdown locations in Table 1 coincide well with the locations of the sudden decrease in the q values (Fig. 8) and those obtained by flow visualization (the open circles in Fig. 8). This coincidence suggests that the magnitudes of u^* and w^* within the vortex core are closely linked to the variations

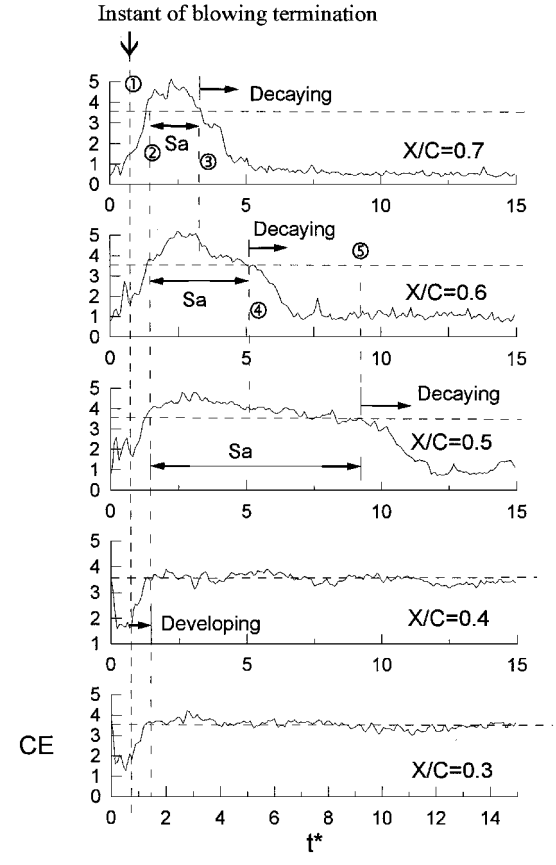

Fig. 9 Time-dependent variations of the integrated CE at various X/C locations. The dashed vertical lines with different numbers denote different evolutionary stages after the transient along-core blowing terminates. The horizontal dashed lines represent the level of CE in the vortex core that never breaks down.

of the q value and the maximum swirl angle ϕ_{max} after the transient along-core blowing is applied.

Physical Interpretation of Stability Parameter and Maximum Swirl Angle

Formation of a stable leading-edge vortex structure over the delta-wing can be interpreted by the concept of vorticity balance.[21] This concept illustrates the balance between the vorticity generated by the separated shear layer from the sharp leading edge and that convected downstream along the vortex core. In response to the transient along-core blowing, the maximum swirl angle ϕ_{max} provides the limitation for the magnitudes of u^* and w^* to maintain a stable vortex core. In addition, the q value represents the ratio of along-core vorticity to the vorticity in the swirling direction.[20] Thus, a higher value of q implies a vortex core having a highly concentrated along-core vorticity component. When the transient along-core blowing is issued from the wing apex, higher values of q and u_c^* will magnify the convection of the along-core vorticity, leading to a more stable vortex core. On the contrary, reduction in the magnitude of q and u_c^* will disrupt the vorticity balance, leading to vortex breakdown. This is the reason why the behavior of the stability parameter q in Fig. 8 is similar to that of u_c^* in Ref. 16.

In other words, the magnitude of u^* within the vortex core responding to the transient along-core blowing must change in accordance with that of w^*. Meanwhile, the magnitudes of u^* and w^* within the vortex core must satisfy the criterion $\phi \leq \phi_{max}$ to balance between the vorticity generation and the vorticity convection along the vortex core. Moreover, the maximum swirl angle ϕ_{max} within the vortex core is found to be nearly the same in the case of transient along-core blowing and in the unperturbed case. Considering the concept of vorticity balance,[21] the maximum swirl angle can be realized as an inherent property for the stable vortex core over a delta-wing at fixed AOA and sweep angle.

Along-Core Pressure Gradient at the Vortex Center

Considering the cylindrical axisymmetric vortex core, the along-core pressure gradient at the vortex center can be related to that on the wing surface and the integrated centrifugal effect (CE)

$$\mathrm{CE} = \int_0^{Rs} \frac{(w^*)^2}{r^*}\,\mathrm{d}r^*$$

by the following equation:

$$\frac{\partial p_c^*}{\partial x} = \frac{\partial p_s^*}{\partial x} - 2\frac{\partial}{\partial x}\left[\int_0^{Rs} \frac{(w^*)^2}{r^*}\,\mathrm{d}r^*\right] = \frac{\partial p_s^*}{\partial x} - 2\frac{\partial}{\partial x}(\mathrm{CE}) \quad (4)$$

The limits of the integration range from the vortex center ($r^* = 0$) toward the location where the maximum swirling velocity occurs (symbolically indicated as Rs). The surface pressure measurements in Refs. 16 and 22 showed that $\partial p_s^*/\partial x$ is positive in the streamwise direction. Thus, Eq. (4) reveals the influence of the integrated CE on the along-core pressure gradient at the vortex center.

After the transient along-core blowing is applied, the time histories of the integrated CE are shown in Fig. 9 for successive X/C locations. The maximum uncertainty of CE estimated from 10 sample runs is around 0.2. During the developing stage (between the vertical lines 1 and 2) and at all X/C locations in Fig. 9, the magnitude of CE increases quickly because the absolute magnitude of w^* increases within the vortex core (refer to Fig. 7 at $z/s = 0.38$, 0.43, and 0.7). In the region $X/C \leq 0.4$ where the vortex core never breaks down, the magnitude of CE remains nearly constant around 3.5–3.8 (the horizontal dashed lines in Fig. 9) after the developing stage (line 2). However, in the region $X/C \geq 0.5$, the magnitudes of CE increase and maintain high values (CE > 3.5–3.8) during the saturation stage (marked by Sa in Fig. 9) and then decrease significantly from the beginning of the decaying stage.

Within the time interval $1.35 < t^* < 3.7$ (between lines 2 and 3), the magnitude of CE downstream of $X/C = 0.5$ shows a positive gradient of CE (namely, $\partial[\mathrm{CE}]/\partial x > 0$). Considering the relation in Eq. (4), the positive gradient of CE becomes a favorable effect to enlarge the favorable pressure gradient along the vortex core in the region $X/C = 0.5$–0.7. This favorable effect coincides with the high values of q at $t^* < 4.1$ (Fig. 8). At $X/C = 0.7$, the magnitude of CE decreases significantly within the time interval $3.7 < t^* < 5.0$ (namely, between lines 3 and 4). This gives $\partial[\mathrm{CE}]/\partial x < 0$ between $X/C = 0.6$ and 0.7. Thus, the negative gradient of CE in Eq. (4) becomes an adverse effect in the region $0.6 < X/C < 0.7$, whereas the favorable effect still exists between $X/C = 0.5$ and 0.6. In Fig. 8 at $t^* = 5.4$, the sudden drop of the q values near $X/C = 0.6$ is an indication of this adverse effect. Similarly, the adverse effect occurs in the time interval $5.0 < t^* < 9.2$ (or between lines 4 and 5), indicating the occurrence of the vortex breakdown between $X/C = 0.5$ and 0.6. In Fig. 8, the occurrence of the sudden drops in the q value coincides well with that of the adverse effect ($\partial[\mathrm{CE}]/\partial x < 0$) derived from Fig. 9. This coincidence implies that the variations in the magnitude of w^* within the vortex core will induce different amounts of the centrifugal effect. The positive or negative streamwise gradient of the integrated effect can create either favorable or adverse effects to the along-core pressure gradient at the vortex center during the complete evolutionary process.

Concluding Remarks

The unsteady vortex structure over a delta-wing with a 75-deg sweep angle and at a 40-deg angle of attack was investigated experimentally after the transient along-core blowing was applied from the wing apex. It was found that the highly sensitive characteristic in the central region of the vortex core occurs not only in the along-core direction but also in the circumferential direction. The analysis of the conical axisymmetric vortex core revealed that, in response to the transient along-core blowing, the magnitude of u^* within the vortex core must change in accordance with that of w^*. Meanwhile, within the stable vortex core, the magnitudes of u^* and w^* must satisfy the stability parameter and the limitation of the maximum swirl angle. In other words, the upstream movement of the vortex breakdown location was dependent on the time-dependent magnitudes of the along-core velocity u^* and the swirling velocity w^* within the vortex core that determine the stability parameter and the swirl angle. The maximum swirl angle $\phi_{\max}$ within the vortex core was found to be nearly the same in the case of transient along-core blowing and in the unperturbed case. This implies that the maximum swirl angle can be realized as an inherent property of the stable vortex core over the delta-wing at fixed AOA and sweep angle. In response to the transient along-core blowing, increasing magnitudes of the along-core and the swirling velocity will overcome the adverse along-core pressure gradient to delay the vortex breakdown and vice versa.

Acknowledgment

The authors are grateful for support from the National Science Foundation of the Republic of China under Grant NSC-85-2212-E-005-006.

References

[1]Polhamus, E. C., "Predictions of Vortex Lift Characteristics by a Leading-Edge Suction Analogy," *Journal of Aircraft*, Vol. 8, No. 4, 1971, pp. 193–199.

[2]Cord, T. T., and Suchomel, C. F., "Supermaneuverability," AIAA Paper 84-2386, March 1984.

[3]Herbst, W. B., "Future Fighter Technologies," *Journal of Aircraft*, Vol. 17, No. 8, 1980, pp. 561–566.

[4]Shi, Z., Wu, J. M., and Vakili, A. D., "An Investigation of Leading-Edge Vortices on Delta-Wing with Jet Blowing," AIAA Paper 88-0504, Jan. 1988.

[5]Bradley, R. G., Whitten, P. D., and Wray, W. O., "Leading-Edge Vortex Augmentation in Compressible Flow," *Journal of Aircraft*, Vol. 13, No. 9, 1976, pp. 238–242.

[6]Campbell, J. F., "Augmentation of Vortex Lift by Spanwise Blowing," *Journal of Aircraft*, Vol. 13, No. 9, 1976, pp. 727–732.

[7]Gu, W., Robinson, O., and Rockwell, D., "Control of Vortices on a Delta-Wing by Leading-Edge Injection," *AIAA Journal*, Vol. 31, No. 7, 1993, pp. 1177–1186.

[8]Helin, H. E., and Watry, C. W., "Effects of Trailing-Edge Jet Entrainment on Delta-Wing Vortices," *AIAA Journal*, Vol. 32, No. 4, 1994, pp. 802–804.

[9]Lee, M., Shih, C., and Ho, C. M., "Response of a Delta-Wing in Steady and Unsteady Flows," *Proceedings of the Forum on Unsteady Flow Separation*, FED Vol. 52, American Society of Mechanical Engineers, New York, 1987, pp. 19–24.

[10]Magness, C., Robinson, O., and Rockwell, D., "Control of Leading-Edge Vortices on a Delta-Wing," AIAA Paper 89-0999, March 1989.

[11]Cipolla, K., and Rockwell, D., "Flow Structure on a Stalled Delta-Wing Subjected to Small Amplitude Pitching Oscillation," *AIAA Journal*, Vol. 33, No. 7, 1995, pp. 1256–1262.

[12]Visbal, M. R., and Gordnier, R. E., "Pitch Rate and Pitch-Axis Location Effects on Vortex Breakdown Onset," *Journal of Aircraft*, Vol. 32, No. 5, 1995, pp. 929–935.

[13]Vorobieff, P., and Rockwell, D., "Multiple-Actuator Control of Vortex Breakdown on a Pitching Delta-Wing," *AIAA Journal*, Vol. 34, No. 10, 1996, pp. 2184–2186.

[14]Lee, M., and Ho, C. M., "Lift Force of Delta-Wing," *Applied Mechanics Review*, Vol. 43, No. 9, 1990, pp. 209–221.

[15]Kuo, C. H., and Lu, N. Y., "Vortex Characteristics over Delta-Wing Subject to Transient Along-Core Blowing," *AIAA Journal*, Vol. 33, No. 12, 1995, pp. 2418–2420.

[16]Kuo, C. H., Lu, N. Y., and Lin, D. C., "Evolution of Vortical Structure over Delta-Wing with Transient Along-Core Blowing," *AIAA Journal*, Vol. 35, No. 4, 1997, pp. 617–624.

[17]Kuo, C. H., and Lin, D. C., "Non-Uniform Recovery of Vortex Breakdown over Delta-Wing in Response to Blowing Along Vortex Core," *Experiments in Fluids*, Vol. 22, No. 1, 1996, pp. 33–44.

[18]Kuo, C. H., and Hsu, C. W., "Development of Vortical Structure over Delta Wing with Leading-Edge Flap," *Journal of Aircraft*, Vol. 34, No. 5, 1997, pp. 577–584.

[19]Faler, J. H., and Leibovich, S., "Disrupted States of Vortex Flow and Vortex Breakdown," *Physics of Fluids*, Vol. 2, No. 9, 1977, pp. 1385–1400.

[20]Lessen, M., Singh, P. J., and Paillet, F., "The Stability of a Trailing Line Vortex, Part I: Inviscid Theory," *Journal of Fluid Mechanics*, Vol. 63, Pt. 4, 1974, pp. 753–763.

[21]Reynolds, W. C., and Carr, L. W., "Review of Unsteady, Driven, Separated Flows," AIAA Paper 85-0527, May 1985.

[22]Roos, F. W., and Kegelman, J. T., "An Experimental Investigation of Sweep Angle Influence on Delta Wing Flows," AIAA Paper 90-0383, Jan. 1990.

F. W. Chambers
Associate Editor